Surfaces, Interfaces and Lubrication

Institution of MECHANICAL ENGINEERS
Journal of MECHANICAL ENGINEERING SCIENCE

Proc IMechE Part C:
J Mechanical Engineering Science
2023, Vol. 237(14) 3236–3246

DOI: 10.1177/09544062221142695
journals.sagepub.com/home/pic
SAGE

Slip at the edge of complete contacts

Daniel J Riddoch and David A Hills

Abstract

We describe an asymptotic method for calculating the size of a zone of partial slip at the edge of a complete contact of arbitrary edge angle and coefficient of friction. Above a critical coefficient of friction the contact remains stuck, and this critical value is explored. A distributed dislocation method is used and the use of different types of numerical quadrature is explored. The size of the slip zone, and its dependence on the contact edge angle and coefficient of friction, are explored.

Keywords

Contact mechanics, interface, frictional slip, complete contacts, asymptotic approach

Date received: 6 July 2022; accepted: 11 November 2022

Introduction

A complete contact is one whose extent is defined by a discontinuity in the gradient profile of one of the contacting surfaces. In layman's terms, this means that the edge of the contact is located at the corner of either of the contacting bodies. This gives rise to a stress singularity at the edge of the contact[1–3] provided that the contact remains intimate throughout the initial contact region, that is, the loading is such that the corner does not lift off. The singularity has to be relieved, and this can be done by plasticity,[4] by the nucleation and propagation of cracks,[5] or by local frictional slip along the contact interface. This contact may persist across then entire interface (i.e. two separate bodies in contact), or it may be a closed pair of crack faces,[6] we consider the former in this case.

It is the last of these effects which we will consider here. The creation of a zone of partial slip is dependent on the loading, as described by Riddoch and Hills[7] the intimate contact must be maintained by the correct signs of the stress intensity factors, and as laid out by Hills and Dini[8] the coefficient of friction must be lower than the value of the traction ratio implied within the dominant eigenvector of the Williams solution.[9]

Calibrations of external loads to the stress intensity factors have shown that the contact will tend to spread outwards under purely normal loading,[7,10,11] so initial investigations focus on outward slip.

Applying Coulomb's friction law throughout, this analysis will endeavour to model the slip and determine the size of the slip zone. Furthermore, previous work has considered only the three-quarter plane problem,[12,13] which applies, for example to the problem of a square block indenting a half-space. In this analysis, this will be extended to consider a variety of indenter angles. Additionally, previously it has been stated that the size of the slip zone, when normalised by a value calculated from the Williams solution, is independent of the coefficient of friction, which has now been found to be incorrect. Figure 1 shows a sketch of the resultant system, with the slip zone present at the edge of contact.

Asymptotic formulation

It has already been mentioned that the Williams solution[9,14] will be used extensively. This provides an asymptotic solution to determine the state of stress in the neighbourhood of the apex of a wedge. This solution places the origin of a polar coordinate system at the edge, a feature which is preserved throughout this analysis.

The state of stress is dominated by two terms, which are the symmetric (here after referred to as mode I) and anti-symmetric (hereafter referred to as mode II) eigensolutions. For a wedge having total internal angle greater than 180^o, the mode I term is

Department of Engineering Science, University of Oxford, Oxford, UK

Corresponding author:
Daniel Riddoch, Department of Engineering Science, University of Oxford, Parks Road, Oxford, Oxfordshire OX1 3PJ, UK.
Email: daniel.riddoch@eng.ox.ac.uk

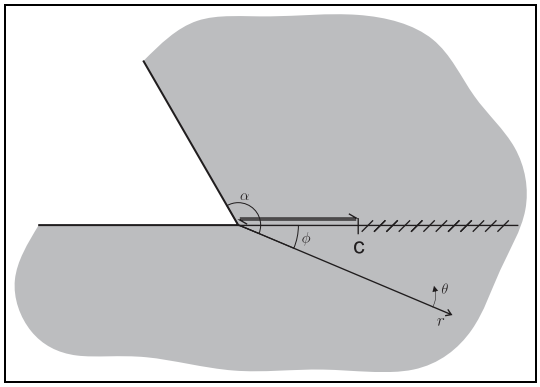

Figure 1. Sketch of a slip zone at the edge of a complete contact of arbitrary internal angle.

singular, and for a wedge having total internal angle greater than 257.4^o, the mode II term is also singular.

The stress is described by the formula

$$\sigma_{ij}(r,\theta) = K_I f_{ij}^I(\theta) r^{\lambda_I - 1} + K_{II} f_{ij}^{II}(\theta) r^{\lambda_{II}-1} \ldots + \text{higher order terms.} \quad (1)$$

where K_I and K_{II} are the mode I and mode II stress intensity factors respectively, f_{ij}^I and f_{ij}^{II} are the mode I and mode II eigenvectors, and λ_I and λ_{II} are the mode I and mode II eigenvalues respectively.

This solution may be used as a bilateral solution, as an adhered complete contact is equivalent to a wedge whose internal angle is the sum of a half-plane and the internal angle of the contacting body. Therefore, this solution can be used as the basis for this analysis. At this stage, we will define two constants, that we find from the Williams solution and which will be useful later.

We begin by recalling the work of Hills and Dini[4] and using this to extract the characteristic length dimension of the problem. Before doing this, however, it will be useful to align the eigensolution of the problem to the slip line with new basis vectors along the interface, as this will allow easier normalisation later on. Quite simply this is done by applying multipliers to the vectors; $K_I^o = K_I f_{\theta\theta}^I(\phi)$, and $K_{II}^o = K_{II} f_{\theta\theta}^{II}(\phi)$, where K_I, K_{II} are the two stress intensity factors, ϕ is the angle of the interface line to the bisector of the combined body, and $f_{\theta\theta}^I, f_{\theta\theta}^{II}$ are the mode I and mode II parts of the $\sigma_{\theta\theta}$ component of the Williams eigenvector, respectively. So, we can now extract our length dimension, denoted by d_0 and defined by

$$d_0 = \left| \frac{K_I^o}{K_{II}^o} \right|^{\frac{1}{\lambda_{II}-\lambda_I}}.$$

The second important quantity we wish to define is the implied size of the slip zone, as indicated by the ratio of the tractions given by the Williams solution. This is the point where $-f_c \sigma_{\theta\theta} = \sigma_{r\theta}$, which is the Coulomb friction law, where f_c is the coefficient of friction. The Williams solution provides this point, which we denote as c_0, given by

$$c_0 = \left(-\frac{(f_c - g_{r\theta}^I) K_I^o}{(f_c - g_{r\theta}^{II}) K_{II}^o} \right)^{\frac{1}{\lambda_{II}-\lambda_I}}. \quad \text{Therefore} \quad (2)$$

$$\frac{c_0}{d_0} = \left(-\frac{f_c - g_{r\theta}^I}{f_c - g_{r\theta}^{II}} \right)^{\frac{1}{\lambda_{II}-\lambda_I}}, \quad (3)$$

where $g_{r\theta}^I = \frac{f_{r\theta}^I(\phi)}{f_{\theta\theta}^I(\phi)}$, and $g_{r\theta}^I = \frac{f_{r\theta}^{II}(\phi)}{f_{\theta\theta}^{II}(\phi)}$, are the eigenvector ratios.

Finally, we will use our inherent length scale (d_0) to normalise the problem. This will allow us to relate problems under different loads or different conditions. Drawing again on the work of Churchman and Hills[10] and Hills and Dini[4] we see that we may write the stresses as

$$\frac{\sigma_{\theta\theta}(r)}{G_0} = \left(\frac{r}{d_0} \right)^{\lambda_I - 1} + \left(\frac{r}{d_0} \right)^{\lambda_{II}-1}, \quad (4)$$

$$\frac{\sigma_{r\theta}(r)}{G_0} = g_{r\theta}^I \left(\frac{r}{d_0} \right)^{\lambda_I - 1} + g_{r\theta}^{II} \left(\frac{r}{d_0} \right)^{\lambda_{II}-1}, \quad (5)$$

where $G_0 = K_I^{o\frac{\lambda_{II}-1}{\lambda_{II}-\lambda_I}} K_{II}^{o\frac{\lambda_I - 1}{\lambda_I - \lambda_{II}}}$.

Dislocation formulation

Turning now to the problem of modelling the actual extent of slip, we require a knowledge of the size of the slip zone, and a method of modifying the stresses. The former will be something we will return to later, but for the latter, we will use dislocations. Crystalline dislocations are used in material science to represent discontinuities in lattice structures, although that is not how we will use them here.

Instead we are interested in the stress and displacement fields that the dislocations create. The form of these is well known and understood[15–18] and will be used extensively. These influence functions are known for a dislocation in an infinite plane, and so a method must be found to determine the influence of such dislocations in a semi-infinite wedge, a system which, as we have said, is analogous to an adhered complete contact. This has been done previously by considering a single dislocation and using distributions of dislocations to clear the free surfaces of induced traction,[19–22] and in this analysis we will use the results calculated by Riddoch and Hills.[22]

Denoting the wedge influence of a dislocation by $\bar{G}_{ijk}(r,\theta,\xi,\rho)$, where i corresponds to the Burgers vector of the dislocation, jk is the stress component under consideration, r is the observation radius from the origin (placed at the edge of contact, or apex of

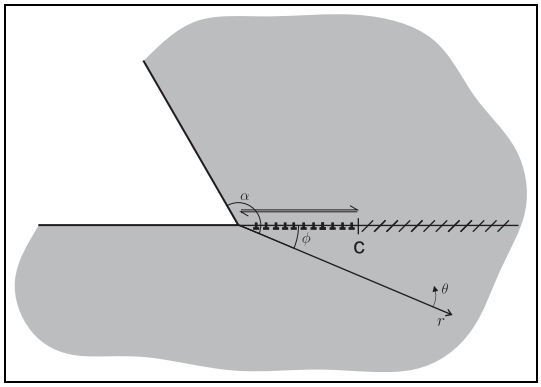

Figure 2. Sketch showing the distribution of dislocations along the slip interface.

the wedge), θ is the observation angle from the wedge bisector, ξ is the radius of the dislocation core from the origin, and ρ is the angle of the dislocation core. We place a distribution of dislocations along the contact interface, from the edge of contact to the actual slip stick boundary, which we denote by c. The density of this distribution is denoted by B_r. This distribution of dislocations is sketched in Figure 2 which shows the dislocations placed along the slip interface of the problem, as shown in Figure 1.

Consequently, the corrected stresses along the contact interface can be written as

$$\frac{\sigma_{r\theta}(r,\phi)}{G_0} = g^I_{r\theta}\left(\frac{r}{d_0}\right)^{\lambda_I-1} + g^{II}_{r\theta}\left(\frac{r}{d_0}\right)^{\lambda_{II}-1} + \ldots \frac{2\mu}{\pi(\kappa+1)}\int_0^c B_r\left(\frac{r}{d_0}\right)\bar{G}_{rr\theta}\left(\frac{r}{d_0},\phi,\xi,\phi\right)d\xi, \quad \text{for } 0\leqslant r\leqslant c, \tag{6}$$

$$\frac{\sigma_{\theta\theta}(r,\phi)}{G_0} = \left(\frac{r}{d_0}\right)^{\lambda_I-1} + \left(\frac{r}{d_0}\right)^{\lambda_{II}-1} + \frac{2\mu}{\pi(\kappa+1)}\ldots \int_0^c B_r\left(\frac{r}{d_0}\right)\bar{G}_{r\theta\theta}\left(\frac{r}{d_0},\phi,\xi,\phi\right)d\xi, \quad \text{for } 0\leqslant r\leqslant c. \tag{7}$$

Within the slip region, the Coulomb friction law must be satisfied, meaning

$$0 = (g^I_{r\theta}-f_c)\tilde{r}^{\lambda_I-1} + (g^{II}_{r\theta}-f_c)\tilde{r}^{\lambda_{II}-1} + \ldots \int_0^c \hat{B}_r(\xi)(\bar{G}_{rr\theta}(\tilde{r},\phi,\xi,\phi) - f_c\bar{G}_r r\theta(\tilde{r},\phi,\xi,\phi))d\xi, \quad \text{for } 0\leqslant r\leqslant c, \tag{8}$$

where $\tilde{r} = \frac{r}{d_0}$ and $\hat{B} = \frac{2\mu}{\pi(\kappa+1)}B$, for values of $0\leqslant r\leqslant c$. Equation 8 is the governing equation, and the solution to this equation will solve the problem fully. There are, however, two unknowns in the problem. The first of these is the dislocation density, and the second is the size of the slip zone c. The first may be found by inverting the integral equation, but the second must be found by some other method.

A numerical inversion

Considering, first, the inversion of the integral equation, we note that we will require a numerical method. This is because the dislocation kernels, as found by Riddoch and Hills[22] do not have a closed-form expression. The kernels are, however, singular in nature, so equation 8 is a Cauchy singular integral equation.

Numerical quadrature

Consequently, a Gauss-Chebyshev quadrature will be employed as described by Erdogan et al.[23] This quadrature deals with the singularity by separating the behaviour into a well-behaved unknown function, denoted by φ, and a fundamental function, denoted ω, which encapsulates the power order singularity, but is well known and can be removed from the equation by use of the quadrature.

The choice of this fundamental function determines the type of behaviour that can be expected of the solution at the end points. However, there are only two types of behaviour which are accounted for, square root singular, and square root bounded, and so with either possible at both ends, giving a total of four different cases, as laid out in Table 2.2 by Hills et al.[24]

We must consider the state of stress at the edge of contact and the slip stick boundary. Considering, first, the latter, in the adhered case, the stress at this point is bounded, with each component's value being a finite number, this will still be true as the contact slips. So here the corrective term must be bounded.

The question is not so easily resolved at the contact edge end of the interval however. The stresses in the bilateral solution are singular at the edge of contact, specifically, they are power order singular, and the power is given by $\lambda_I - 1$. When the interface is slipping the form may not immediately be so obvious. However, at a very local level, for $r << c$, the tractions will be similar in form to those which arise when the contact is in full sliding. The nature of the tractions when the contact is sliding is known, and they are asymptotically described by a power order singular term, with order $\lambda_s - 1$, where λ_s is an eigenvalue solution, as described by Conminou.[25] We have generally that $\lambda_I \neq \lambda_s$, and $0 < \lambda_I < 1, 0 < \lambda_s < 1$ so we can say that, for any $L > 0$, there exists $\epsilon > 0$ such that $|\epsilon^{\lambda_I-1} - \epsilon^{\lambda_s-1}| > L$. This is fairly trivially proven, and hence no proof is provided here. The implication of this however, is that the difference between the adhered and sliding solutions grows without bound as r approaches 0, the edge of contact. Therefore, a singular behaviour at the edge of contact is expected.

Applying singular-bounded quadrature

Consequently, a singular-bounded quadrature is employed. It should be noted that this is the same quadrature as was applied by Churchman and Hills.[12] Table 2.2 (case II) in Hills et al.[24] then gives us a method for choosing our collocation and integration points.

Before we can apply the quadrature, we must first transform the integral. The quadrature requires the integration range to be $[-1, 1]$, so we must find a transformation from the current range $[0, c]$. This is achieved fairly easily by the applying the transform $\tilde{r} = \frac{c}{2}(s+1)$, for the collocation points, and $\xi = \frac{c}{2}(t+1)$ for the integration points. It is useful at this stage to note that $\frac{d\xi}{dt} = \frac{c}{2}$.

Applying these substitutions gives us the integral equation

$$\begin{aligned}(g^I_{r\theta} - f_c)\left(\frac{c}{2}(s+1)\right)^{\lambda_I - 1} + (g^{II}_{r\theta} - f_c)\left(\frac{c}{2}(s+1)\right)^{\lambda_{II}-1} \\ + \ldots \int_{-1}^{1} \hat{B}_r(t)\left(\bar{G}_{rr\theta}\left(\frac{c}{2}(s+1), \phi, \frac{c}{2}(t+1), \phi\right)\right. \\ \left. -\ldots f_c \bar{G}_{r\theta\theta}\left(\frac{c}{2}(s+1), \phi, \frac{c}{2}(t+1), \phi\right)\right)\frac{c}{2}dt = 0, \\ \text{for} -1 \leqslant s \leqslant 1.\end{aligned} \tag{9}$$

At this point it is worth noting that generally $G_{ijk}(r, \theta, \xi, \rho) = \frac{1}{\gamma} G_{ijk}(\gamma r, \theta, \gamma\xi, \rho)$, so we may rearrange the equation to find

$$\begin{aligned}(f_c - g^I_{r\theta})\left(\frac{c}{2}(s+1)\right)^{\lambda_I - 1} + (f_c - g^{II}_{r\theta})\left(\frac{c}{2}(s+1)\right)^{\lambda_{II}-1} \ldots \\ = \int_{-1}^{1} \hat{B}_r(t)(\bar{G}_{r\theta\theta}(s+1, \phi, t+1, \phi) - \ldots \\ f_c \bar{G}_{rr\theta}(s+1, \phi, t+1, \phi))dt, \qquad \text{for} -1 \leqslant s \leqslant 1.\end{aligned} \tag{10}$$

This equation is now in a form where the quadrature may be applied. This leads us to a set of N simultaneous equations in N unknowns, which are described by

$$\begin{aligned}(f_c - g^I_{r\theta})\left(\frac{c}{2}(s_k+1)\right)^{\lambda_I - 1} + (f_c - g^{II}_{r\theta})\left(\frac{c}{2}(s_k+1)\right)^{\lambda_{II}-1} \ldots \\ = \sum_{i=1}^{N} W_i \varphi(t_i)(\bar{G}_{r\theta\theta}(s_k+1, \phi, t_i+1, \phi) - \ldots \\ f_c \bar{G}_{rr\theta}(s_k+1, \phi, t_i+1, \phi))\end{aligned} \tag{11}$$

where W_i is the weight function described by Hills et al.[24] and φ is such that $\omega(s)\varphi(s) = B_r(s)$, with ω the fundamental function also described by Hills et al. The values $\varphi(t_i)$ are the N unknowns which we solve the equations for.

Table 1. Table of conditions in the slip and stick regions.

	Slip region	Stick region
Tractions	$\lvert\sigma_{r\theta}(r)\rvert = f_c\sigma_{\theta\theta}(r)$(A)	$\lvert\sigma_{r\theta}(r)\rvert < f_c\sigma_{\theta\theta}(r)$(B)
Displacements	$\text{sgn}(h(r)) = \text{sgn}(\sigma_{r\theta}(r))$(C)	$h(r) = 0$(D)

The size of the slip zone

Having in hand this inversion method, we now come to solve the set of equations. By use of the transforms, this requires knowledge of the size of the slip zone c. No condition has been explicitly set out for this, and the problem is fully specified.

Two constraints. Previous studies[12,13] have utilised a pair of conditions to calculate the size of the slip zone. This is done by guessing the size of the slip zone, and then checking these conditions to ensure that the estimated slip zone size satisfies both.

These conditions are derived from two basic phenomena. The first of these is that Coulomb's law is satisfied at a given point if and only if the point is in the slip region. For a point within the slip region, as specified by equation 8, this condition will be automatically satisfied by any solution to equation 8. Points outside of the slip zone satisfy this condition:

$$|\sigma_{r\theta}(r)| < f_c\sigma_{\theta\theta}(r), \quad \text{for } r > c, \quad \text{with } \sigma_{\theta\theta}(r) < 0. \tag{12}$$

The second condition within the slip region is derived from the orthogonality condition. This requires the velocity of a slipping point to have the same sign as the shear stress at that point. As this analysis is quasi-static in nature, we do not have a rigorous definition of velocity. However, it is a sufficient approximation to consider instead the slip displacement. Slip displacement is defined as the integral of the dislocation density, since the dislocations themselves represent the displacement discontinuity. We may write this condition as

$$\begin{aligned}\text{sign}(h(r)) : &= \text{sign}\left(\int_0^r B_r(\xi)d\xi\right) = \text{sign}(\sigma_{r\theta}(r)) \\ &\text{for } 0 \leqslant r \leqslant c.\end{aligned} \tag{13}$$

We now have four conditions, summarised in Table 1. The first of these, condition A, is automatically enforced by the solution of the integral equations. Similarly, the last of these, condition D, is automatically true; no dislocations are present along the interface in the stick region and so no displacement is caused. We can, however, use the remaining two conditions, B and C, to constrain the solution.

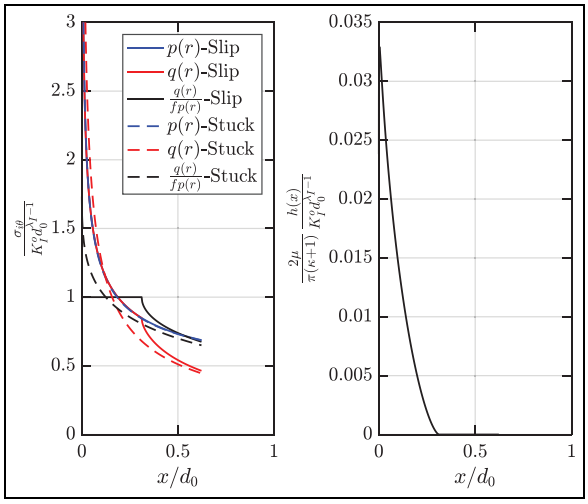

Figure 3. Plot of the stresses in a slipping square edge indenter with a slip zone of size $c = 2.5c_0$.

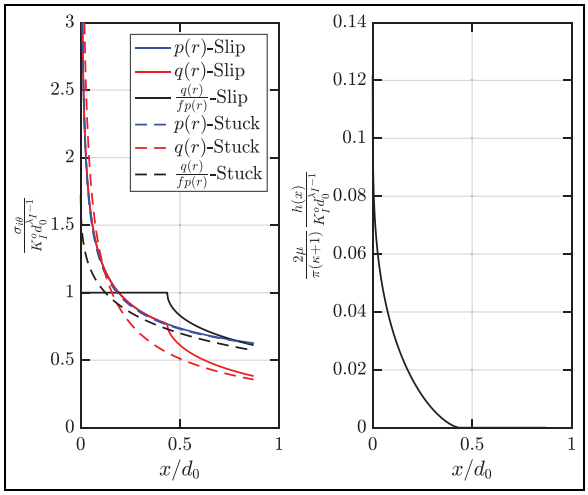

Figure 4. Plot of the stresses in a slipping square edge indenter with a slip zone of size $c = 3.5c_0$.

These place restrictions on the solution in the slip region and the stick region, and it may appear that these conditions are sufficient.

Experience has shown that in this case, the conditions, whilst necessary, are not sufficient to define a unique size for the slip zone. Figure 3 shows the stresses implied by a slip zone which is too small, according to our findings later in the "Results" section. It can be observed that both conditions described here are satisfied, the left hand plot shows (solid black line) that no slip is implied in the slip region. Furthermore, it can easily be observed that both the shear traction (solid red line) and the slip displacements(right hand plot) are positive throughout the slip zone. This would therefore appear to be a valid solution.

Figure 4 shows the stress in the same contact, but in this case we specify a slip zone size that we believe to be too large. Once again, it can be observed that

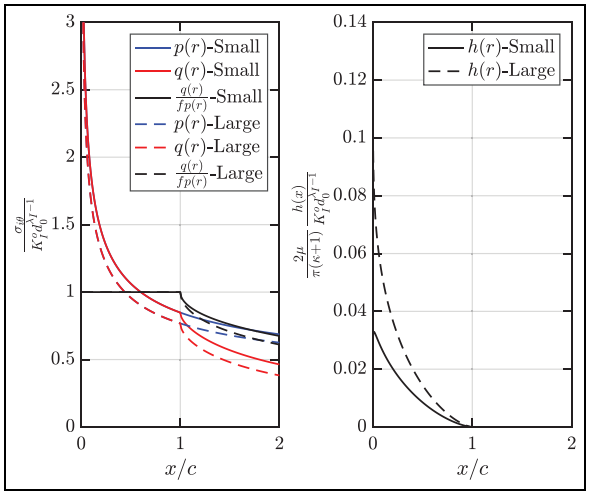

Figure 5. Overlay plot showing the stresses produced for two different slip zone sizes, small being $c = 2.5c_0$, and large being $c = 3.5c_0$.

there is no violation of the slip condition in the stick region (solid black line, left hand plot) and that slip displacement and shear stress have the same sign (right hand plot and solid red line, left hand plot respectively.) So this too would appear to be a valid solution.

This is obviously problematic, the constraints are not only providing multiple solutions, but rather a range. Experience shows for example that for $c = 100c_0$, both conditions are still satisfied. So, given the correct solution is not given by the minimum viable solution, nor the maximum, but rather some point in the middle, we must utilise other constraints to determine the solution. This is made more difficult by the fact that the state of stress is qualitatively similar for both cases, as is highlighted in Figure 5 which overlays the stresses found for each of these cases.

The sliding solution. As previously mentioned by Churchman and Hills[12] it may be useful to consider the solution for a sliding block, as developed by Conminou.[25] This gives rise to an eigenvalue, denoted λ_s, calculated by finding the solution to

$$0 = \cos(\pi\lambda_s)(\sin(\lambda_s\phi)^2 - \lambda_s^2\sin(\phi)^2) + \ldots \quad \frac{\sin(\pi\lambda_s)(\sin(2\lambda_s\phi) + \lambda_s\sin(2\phi))}{2} + \ldots \tag{14}$$

$$f_c\sin(\pi\lambda_s)(\lambda_s(1+\lambda_s)\sin(\phi)^2). \tag{15}$$

However, the sliding asymptote is valid only for a very small region of the slip zone. We do not have to hand, a bound of the range of validity of this solution, so we cannot say with any confidence that this approximation will be accurate at any point a finite distance from the contact edge. The solution is exact

only when $r << c$, or $\frac{r}{c} \to 0$, neither of which gives a quantifiable value of r, below which the solution is always valid, or above which the solution is never valid. It is therefore difficult to enforce conditions based on this approximation.

Slip displacements

The orthogonality condition requires the calculation of the slip displacements, which must be of the same sign as the shear stress. It is tempting to find other conditions. Perhaps the most obvious of these to consider is the prevention of a turning point in the slip displacements. Intuitively it may seem that the slip displacements must be strictly increasing from the slip stick boundary to the edge of contact.

However, this statement has been made without justification, and no immediate justification is apparent. Slip displacements are calculated from dislocation densities, and hence reference discontinuities, so no relation between the stress and the strain may be drawn. So, whilst it may appear at first sight to be obvious, we cannot say with any certainty that this will be the case, and so we can not enforce a condition based on this assumption.

Similarly, it could be argued that the slip displacement should not show singular behaviour at the edge of contact either. It is tempting therefore to enforce the condition that the minimum value of the second derivative of slip displacement with respect to position is bounded at the edge of contact. In practical terms this would mean that the slip length at which this value is minimised would be the true slip length. However, this is once again making assumptions about the form of the slip displacements, which cannot be rigorously justified. It is, therefore, not possible to strictly enforce any constraints on the slip displacements, beyond the use of the orthogonality condition.

An alternative numerical approach

All of the problems described above present a serious obstacle to accurately determining the size of the slip zone. Let us consider a different approach. Earlier, we described at length, how and why we chose the singular bounded quadrature. Let us now consider an alternative conclusion.

The choice of end point behaviour forces a choice between square root singular and square root bounded. The reason that we are forced to make this choice is so that any singular behaviour can be separated. This means that we have one function whose form is known precisely (the fundamental function) and the other part of the function, φ, which is unknown, well behaved, and allows us to sample at chosen points without worrying about singular behaviour being missed. However, if the power order behaviour of the solution is not close to $\pm\frac{1}{2}$, then φ will display behaviour that is either near singular or near bounded.

For this reason, when we find that the power order behaviour of the solution is not close to either square root bounded or square root singular, but rather lies somewhere in between, particularly if the behaviour is weakly singular (i.e. of power order much smaller than square root) we can investigate the behaviour as if the problem is bounded.

We may employ the bounded-bounded quadrature when investigating the slip problem. The power order behaviour of the corrective term will be of order $\lambda_s - \lambda_I$, but this is not close to square root singular. So we apply the same transformations as we did for the singular-bounded case, albeit with the selection of collocation, integration and weights being from the bounded-bounded type. This gives us $N+1$ equations in N unknowns, given by

$$\begin{aligned}&(f_c - g^I_{r\theta})\left(\frac{c}{2}(s_k+1)\right)^{\lambda_I - 1} + (f_c - g^{II}_{r\theta})\left(\frac{c}{2}(s_k+1)\right)^{\lambda_{II}-1} \ldots \\ &= \sum_{i=1}^{N} W_i \varphi(t_i)(\bar{G}_{rr\theta}(s_k+1,\phi,t_i+1,\phi) - \ldots \\ &f_c \bar{G}_{r\theta\theta}(s_k+1,\phi,t_i+1,\phi)).\end{aligned} \tag{16}$$

This is a fact that we will use to our advantage later; for now though it presents a problem. The method of solution for these equations is to invert a coefficient matrix. This is only possible if the matrix to be inverted is square. So, the way we tackle this problem is to select one of the equations arbitrarily and remove it. This leaves us N equations, and the system is invertible once again. This of course is an approximation, but provided that N is sufficiently large (in practice anything larger than about 30 appears sufficient) this is an appropriate approximation to make.

Determining the size of the slip zone

Now having the inversion method in hand, we must now determine the true size of the slip zone. Once again this cannot be done using pre-existing conditions, and so an estimate must be used and refined. We still use the friction law (equation (12)) and the orthogonality condition (equation (13)) as these conditions must still be fulfilled. Once again, though, these conditions prove necessary but not sufficient.

However, we have another condition that we can utilise. The equation which we discarded when inverting the system must still be satisfied. This is a far stricter condition, and enforces the friction law at the point described by the equation. In practice, this equation is written as

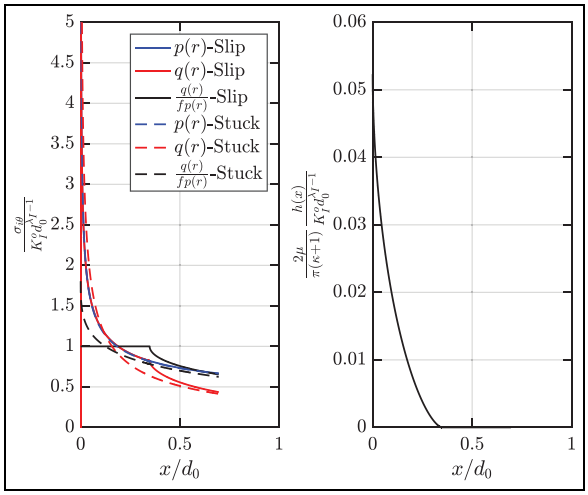

Figure 6. Plot showing the tractions along the slip interface before (dotted) and after (solid) slip, and the slip displacements for a square block indenting a half-space with the coefficient of friction being 0.3.

$$
\begin{aligned}
&- (f_c - g^I_{r\theta})\left(\frac{c}{2}(s_k + 1)\right)^{\lambda_I - 1} - \ldots \\
&(f_c - g^{II}_{r\theta})\left(\frac{c}{2}(s_k + 1)\right)^{\lambda_{II} - 1} + \ldots \\
&\sum_{i=1}^{N} W_i \varphi(t_i)(\bar{G}_{rr\theta}(s_k + 1, \phi, t_i + 1, \phi) - \ldots \\
&f_c \bar{G}_{rr\theta}(s_k + 1, \phi, t_i + 1, \phi)),
\end{aligned}
$$

and the value of this expression is minimised. This gives us the slip zone size which satisfies the friction law at this point, which is therefore, the true size of the slip zone.

Results

Throughout these results, the primary output will be the size of the slip zone c. For ease of comparison, this will always be normalised, either by the initial guess for the size of the slip zone determined from the "full stick" solution and violation of friction law, c_0, or by the problem's inherent length dimension, d_0.

Let us first examine the problem of a square block indenting a half plane. This problem has previously been solved by Churchman and Hills[12] who suggested that the ratio $\frac{c}{c_0} = 2.4$, and does not vary with the coefficient of friction. However, several issues have been found with this work, as discussed by Riddoch and Hills[22] and here in " Two Constraints" section. Consequently, we do not believe this result to be accurate, and we have found that for a coefficient of friction of $f_c = 0.3$, the correct value is $\frac{c}{c_0} = 2.79$, to three significant figures. Figure 6 shows the stresses that this solution implies and the slip displacements. It can clearly be seen that both constraints are satisfied.

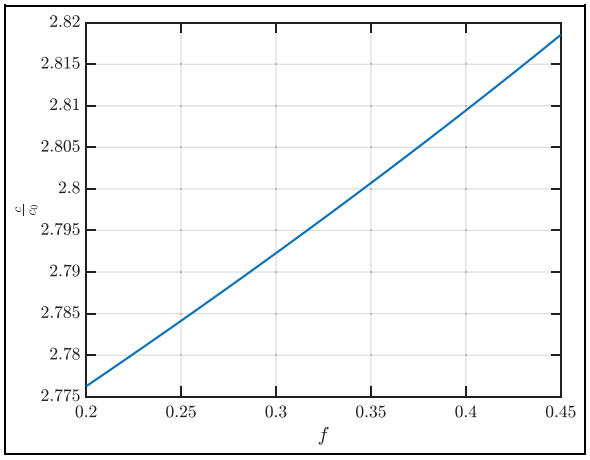

Figure 7. Plot showing the variation of slip zone size for a square block indenting a half-space for varying coefficients of friction.

The next question we then ask is, "Was Churchman right to say that the ratio $\frac{c}{c_0}$ is invariant with friction?" Again, our results would suggest that this is not true. However, the dependence is weak. Figure 7 shows how that ratio $\frac{c}{c_0}$ varies for the above problem when we vary the coefficient of friction between $0.2 \leqslant f_c \leqslant 0.45$. These values are chosen carefully: for very small coefficients of friction, the slip zone will be very large, and thus it risks moving out of the range of validity of the asymptotic solution. On the other hand, for large coefficients of friction there will be a very small slip zone. Hills and Dini[8] found a bound on this, and as we approach it the size of the slip zone becomes sufficiently small for problems to arise, as discussed later in this section.

Next we come to the issue of varying the angles of the contact defining block involved. In practice it is unlikely that two sharp corners would meet perfectly, thus meaning that it makes most sense to consider a block of differing angle indenting a half-space. Furthermore, any slip displacements will destroy the nature of the contact. The method described can tackle such problems, although they are of little practical interest. It is worth noting, however, that in the case where the contacting bodies have the same geometry so the contact interface is colinear with the wedge bisector, then no slip will occur, as by definiton only mode I stresses are present, in which case the ratio of shear to normal stress is invariant with distance from the origin.

Returning to the problem of a block indenting a half-plane, turning now to the result when we vary the angle of the indenter between 0.45π and 0.55π, Figure 8 shows how the ratios $\frac{c}{c_0}$ and $\frac{c}{d_0}$ vary. We have continued to use α to quantify the variation of the angle, although in fact what we vary is the internal angle of the indenter. This is because several bounds exist on the viable solution region, and these are most easily expressed using α.

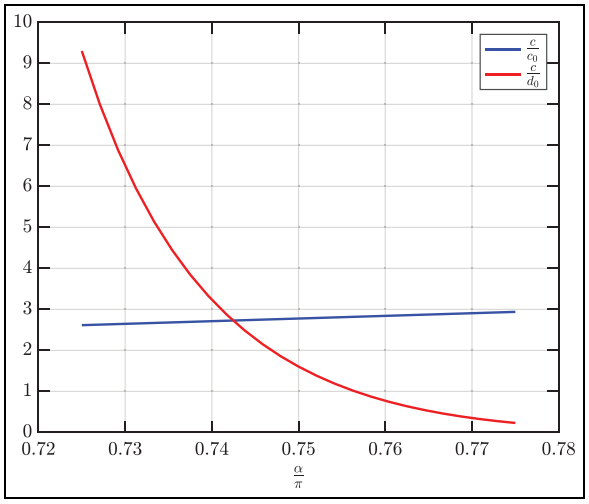

Figure 8. Plot showing the variation of slip zone size for block of various internal angles indenting a half-space.

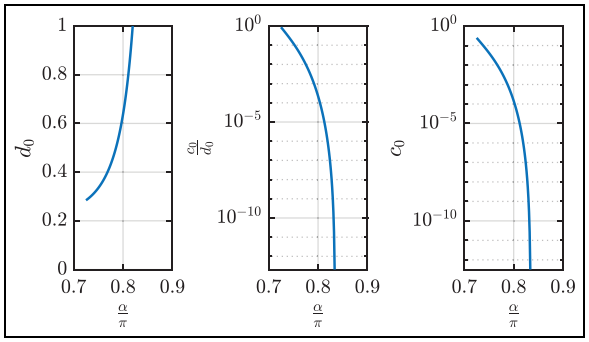

Figure 9. Plot showing the variation of d_0, $\frac{c_0}{d_0}$ and c_0 with angle α.

The first of these bounds is that the mode *II* eigensolution remains singular in nature. This is only the case provided that $\lambda_{II} < 1$, this is true only for $2\alpha > \approx 257^o = 1.4278\pi^c$. The second constraint is related to the value of c_0, whose value depends on the coefficient of friction and the wedge angle, through the properties of the dominant eigenvector. As can be seen in Figure 9 as we let α approach 0.8π, the values of both c_0 and $\frac{c_0}{d_0}$ approach 0. This means two things; firstly it means that any small numerical error becomes very significant; and secondly it means that the gradient of the stress ratio is small.

When the ratio $\frac{c_0}{d_0}$ is small, the Williams solution is dominated by mode *I* terms. This means, as a first order approximation, that we may consider the stresses to be given by just the mode I term,

$$\sigma_{ij}(r) = K_I f_{ij}^I r^{\lambda_I - 1},$$

meaning that the stress ratio is given by

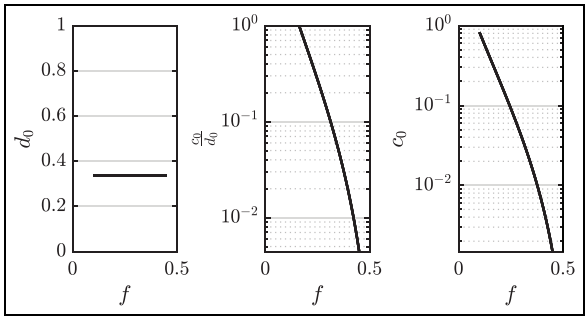

Figure 10. Plot showing the variation of d_0, $\frac{c_0}{d_0}$ and c_0 with coefficient of friction.

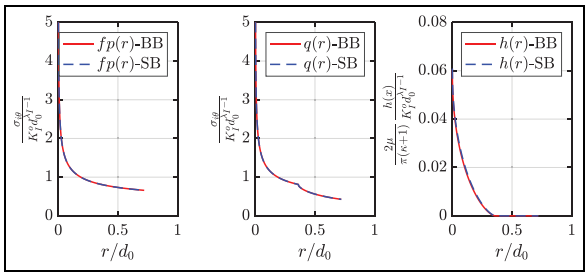

Figure 11. Plot showing an overlay of the stresses calculated using the bounded-bounded (red) and singular-bounded (blue, dashed) quadratures.

$$\frac{\sigma_{r\theta}(r)}{\sigma_{\theta\theta}(r)} = \frac{K_I f_{r\theta}^I r^{\lambda_I - 1}}{K_I f_{\theta\theta}^I r^{\lambda_I - 1}} = \frac{f_{r\theta}^I}{f_{\theta\theta}^I},$$

and is thus invariant with r, over the range where the second term really can be neglected. In practice, of course, there will be an influence from terms in the expansion other than the mode I terms, but that term will dominate, and hence the stress ratio will be nearly constant. This means that any small pertubation, in either the coefficient of friction or the angle, will lead to a large change in the apparent value of c_0.

The variation of d_0, c_0, and $\frac{c_0}{d_0}$, with the angle is shown in Figure 9, and their variation with the coefficient of friction is shown in Figure 10, although d_0 does not vary with coefficient of friction.

Comparison of inversion methods

As we progress with the bounded-bounded quadrature, it is perhaps wise to check that the results that we get using this method are not dissimilar to those found using the singular-bounded quadrature, when supplying that method with the correct size for the slip zone. Figure 11 shows an overlay plot of the stresses and slip displacements for the two methods for a square indenter with coefficient of friction $f_c = 0.3$. As can be seen, the results are almost identical for the

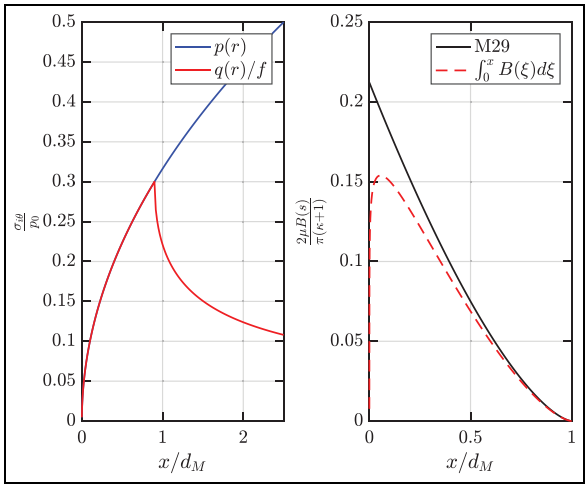

Figure 12. Plot showing the surface tractions (left hand plot) and slip displacement (right hand plot) for a slipping incomplete contact with a slip zone 90% of the true size.

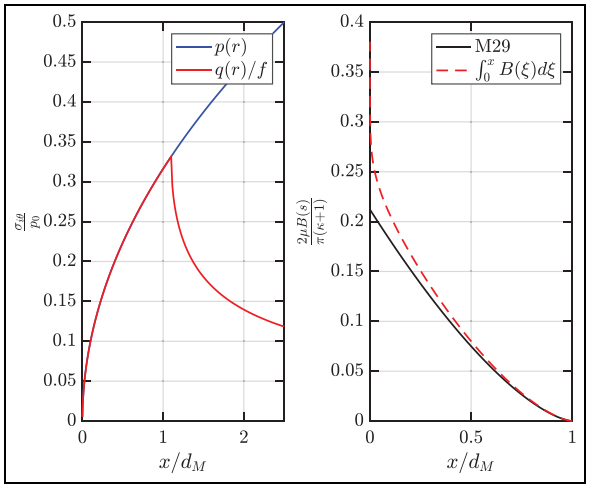

Figure 13. Plot showing the surface tractions (left hand plot) and slip displacement (right hand plot) for a slipping incomplete contact with a slip zone 110% of the true size.

stresses, and the offset is only very marginally different for the slip displacements. This gives us confidence in the correctness and value of the method introduced, as the choice appears to have very little influence on the calculated result.

Discussion

These results are satisfactory and make sense on an intuitive level. However, so far several problems have been left open in this analysis. The first of these, that we will discuss is, "Why are the two conditions which previously were sufficient, now only necessary, these being the friction law and orthogonality conditions?"

In attempting to answer this question, let us consider briefly a different problem. Consider the problem of an semi-infinite incomplete contact, loaded so as to produce a zone of partial slip at the contact edge. These problems are not the same: the incomplete contact is uncoupled, that is changes in the normal traction or normal load will not affect the shear traction and vice versa. Secondly, the contact pressure is square root bounded at the contact edge. The adhered shear traction is square root singular, and we may use a distribution of dislocations to apply a corrective term to model slip.

Happily, on this occasion, a simpler dislocation kernel may be used, and Moore et al.[26] were able to find a closed form solution by inverting the integral equation. This also gives us a true size for the slip zone. However, using a dislocation formulation, we can observe the state of stress generated if the modelled slip zone size is forced to be either too small or too large.

We denote the size of the slip zone calculated by Moore et al. as d_M.Figure 12 shows the surface tractions and slip displacements calculated for a slip zone 90% of the true slip zone size. It can readily be seen that both the friction law and orthogonality conditions are fulfilled here. Similarly Figure 13 shows the same tractions and displacements for a slip zone 110% the true size, once again both conditions are fulfilled. Whilst in neither case does the form of the slip displacement calculated (dashed red line) match that which is found analytically (solid black line), neither case violates any of the conditions we are able to set out. The slip displacements in these plots being calculated by integrating equation 29 in the paper by Moore et al.[26]

For all the reasons previously stated, these problems are not the same, and the behaviour of the stresses is very different, most notably the corrected solution is not singular. However, it is noteworthy that the same problems arise when trying to determine slip zone size in another semi-infinite contact, using the same friction law and orthogonality conditions.

Sliding asymptote

We have already stated that the sliding solution may not be used to constrain the slip solution with any confidence as we are not able to say over what range the asymptotic representation is correct. Even once we have a solution that we are happy with this is a difficult problem, as we do not have values for the sliding stress intensity factor.

However, the sliding asymptote may be fitted to our slip traction at the edge of contact, where an accurate representation is expected. Doing this will obviously result in a very good match at the points which we use for the fit, but it is instructive nevertheless, as it gives an indication of how good an approximation the sliding asymptote is throughout the slip region.

Figure 14 shows a comparison of the tractions found using our method described above and the

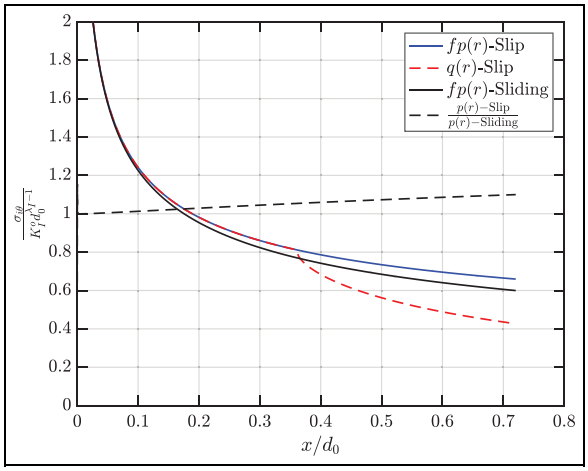

Figure 14. Plot showing a comparison of the slip and sliding tractions.

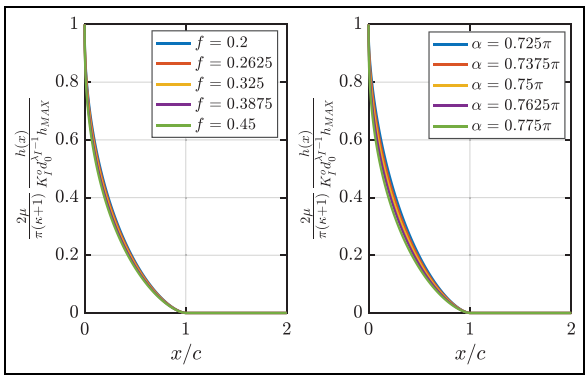

Figure 15. Plot showing a normalised overlay of the slip displacements for different coefficients of friction (left hand plot) and indenter angles (right hand plot).

sliding asymptote, fitted at the edge of contact. The ratio between the two (Figure 14, dashed black line) is particularly instructive as it shows that the asymptotic approximation remains close to the calculated traction for a large portion of the slip region.

Slip displacements

When discussing the slip displacements calculated using the singular bounded quadrature, we stated that we are unable to exclude the possibility of a turning point in the slip displacement, but in all cases examined so far no turning point has been present. So the question may be asked, does a turning point arise, or, as expected, is no turning point present?

Figure 15 shows a normalised overlay of the slip displacements found for five different cases for the coefficient of friction (left hand plot) and for five different angles (right hand plot). It can be seen that the form of each of these is broadly similar, and none displays a turning point behaviour. This is by no means a rigorous proof, or an exhaustive examination, but it is indicative that it seems extremely unlikely that a turning point in slip displacement might be observed.

Conclusion

In this analysis, we have determined the size of a zone of partial slip at the edge of a complete contact. We have shown how the size of this slip zone varies with changes in the coefficient of friction, and the contact angle. This includes a correction of previously published results. Furthermore, bounds have been placed on the range of validity of the asymptotic solution, and/or the existence of a slip region.

Additionally, we have discussed and explored two different numerical methods, and the reasons for choosing either method. Previous conditions used to determine the size of the slip zone have been investigated, and have proved insufficient. Alternative constraints have been explored and ruled out, although these are shown to also be true, but not enforceable as constraints. Finally, a method is arrived at using a feature of one of the numerical methods, although the choice of numerical quadratures has been shown not to affect the solution.

Declaration of conflicting interests

The author(s) declared no potential conflicts of interest with respect to the research, authorship, and/or publication of this article.

Funding

The author(s) disclosed receipt of the following financial support for the research, authorship, and/or publication of this article: Both authors thank Rolls-Royce plc and the EPSRC for the support under the Prosperity Partnership Grant 'Cornerstone: Mechanical Engineering Science to Enable Aero Propulsion Futures', Grant Ref: EP/R004951/1.

ORCID iD

Daniel J. Riddoch https://orcid.org/0000-0002-3991-0947

References

1. Barber J. *Contact mechanics*. Springer, Springer Dordrechet Heidelberg London New York 2018.
2. Johnson KL. *Contact mechanics*. Cambridge: Cambridge University Press, 1987.
3. Dundurs J and Lee MS. Stress concentration at a sharp edge in contact problems. *J Elast* 1972; 2(2): 109–112.
4. Hills DA and Dini D. Characteristics of the process zone at sharp notch roots. *Int J Solids Struct* 2011; 48(14–15): 2177–2183.
5. Riddoch DJ, Cwiekala N and Hills DA. Dislocations in an arbitrary angle wedge. Part ii: Cracks in the wedge. *J Strain Anal Eng Des* 2022; 57: 433–444.
6. Spagnoli A, Carpinteri A and Terzano M. Mode ii crack shielding in a compressed rough crack with friction. *Theor Appl Fract Mech* 2020; 107: 102515.

7. Riddoch DJ and Hills DA. Necessary conditions for near-edge stick of complete contacts. *J Strain Anal Eng Des* 2020; 55(5–6): 172–180.
8. Hills DA and Dini D. What level of friction guarantees adhesion in a complete contact? *J Strain Anal Eng Des* 2004; 39(5): 549–551.
9. Williams ML. Stress singularities resulting from various boundary conditions in angular corners of plates in extension. *J Appl Mech* 1952; 19(4): 526–528.
10. Churchman CM and Hills DA. General results for complete contacts subject to oscillatory shear. *J Mech Phys Solids* 2006; 54(6): 1186–1205.
11. Spagnoli A, Carpinteri A and Terzano M. Near-tip stress fields of rough and frictional cracks under mixed-mode loading. *Fatigue Fract Eng Mater Struct* 2018; 41(10): 2099–2109.
12. Churchman CM and Hills DA. Slip zone length at the edge of a complete contact. *Int J Solids Struct* 2006; 43(7-8): 2037–2049.
13. Paynter RJ, Hills DA and Dini D. Separation and slip at the edge of a complete contact: an asymptotic solution. *Int J Solids Struct* 2010; 47(18-19): 2613–2619.
14. Barber JR. *Elasticity*. Dordrecht: Springer, 2010.
15. Worden RE and Keer LM. Green's functions for a point load and dislocation in an annular region. *J Appl Mech* 1991; 58: 954–959.
16. Dundurs J and Mura T. Interaction between an edge dislocation and a circular inclusion. *J Mech Phys Solids* 1964; 12(3): 177–189.
17. Lee MS and Dundurs J. Edge dislocation in a surface layer. *Int J Eng Sci* 1973; 11(1): 87–94.
18. Nowell D and Hills DA. Open cracks at or near free edges. *J Strain Anal Eng Des* 1987; 22(3): 177–185.
19. Hecker M and Romanov AE. The stress fields of an edge dislocation near a wedge-s haped boundary. *Phys Status Solidi (A)* 1992; 130(1): 91–101.
20. Hecker M and Romanov AE. The stress fields of edge dislocations near wedge-shaped boundaries and bonded wedges. In: Kostorz G, Calderon HA and Martin JL (eds) *Fundamental aspects of dislocation interactions*. Amsterdam: Elsevier, 1993, pp.411–414.
21. Churchman CM, Korsunsky AM and Hills DA. The edge dislocation in a three-quarter plane. Part i: Influence functions. *Eur J Mech A/Solids* 2006; 25(1): 42–50.
22. Riddoch DJ and Hills DA. Dislocations in an arbitrary angle wedge. Part i: the dislocation kernel. *J Strain Anal Eng Des* 2022; 57: 476–483.
23. Erdogan F, Gupta GD and Cook T. Numerical solution of singular integral equations. In: Sih GC (ed.) *Methods of analysis and solutions of crack problems*. Dordrecht: Springer, 1973, pp.368–425.
24. Hills DA, Kelly PA, Dai DN, et al. *Solution of crack problems: the distributed dislocation technique*. Singapore: Springer Science & Business Media, 2013. Vol. 44.
25. Comniou M. Stress singularity at a sharp edge in contact problems with friction. *J Appl Math Phys* 1976; 27: 493–499.
26. Moore MR, Ramesh R, Hills DA, et al. Half-plane partial slip contact problems with a constant normal load subject to a shear force and differential bulk tension. *J Mech Phys Solids* 2018; 118: 245–253.